TM No.
771160

NAVAL UNDERWATER SYSTEMS CENTER
NEW LONDON LABORATORY
NEW LONDON, CONNECTICUT 06320

(9) Technical Memorandum

(6) THE INVERSE FAST FIELD PROGRAM (IFFP): AN APPLICATION TO THE DETERMINATION OF THE ACOUSTIC PARAMETERS OF THE OCEAN BOTTOM*

(11) Date: 5 Aug 1977

(12) 23p.

Prepared by: F. R. DiNapoli
F. R. DiNapoli
Special Projects
Department

(10) F. R. /DiNapoli

(14) NUSC-TM-771160

(16) F52552

(17) SF52552601

*Presented at the 9th I.C.A. Madrid, Spain 7/5/77

405 918

JOB

ABSTRACT

The problem of estimating the acoustic field produced by a point source located in an environment which is arbitrarily stratified with depth only has received considerable attention. Various models exist which provide reasonable results provided sufficient information about the environment and source characteristic is available. This paper is concerned with solving for the inverse of this problem, i.e., information about the environment, in particular the impedance at the ocean-bottom interface is sought from a knowledge of the received acoustic field and the source which produced it. The theoretical formulation of the scheme is presented and its numerical implementation is discussed and illustrated for three examples of successive orders of environmental complexity.

ADMINISTRATIVE INFORMATION

This document was prepared under NUSC Project No. A65002 Navy Subproject No. SF 52 552 601-19325, "Underwater Acoustical Environmental Modeling and Data Bank for Sonar System Design and Performance Prediction," Principal Investigator, Dr. F. R. DiNapoli (Code 3123). The sponsoring activity is the Naval Sea Systems Command (SEA 0641-4), A. P. Franceschetti, Program Manager.

The author of this memorandum is located at the Naval Underwater Systems Center, New London Laboratory, New London, Connecticut 06320.

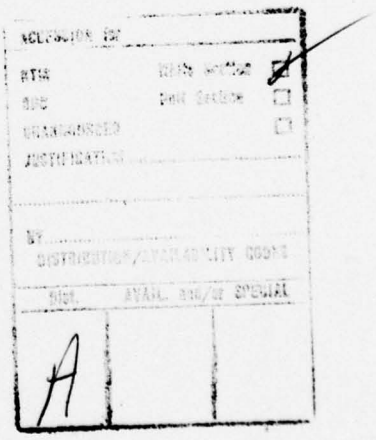

Although the subject of this paper is the inverse solution we will begin with a discussion of the direct solution because it came first chronologically and its success provided the motivation for the development of the inverse solution.

By direct solution, figure 1, we mean that situation where the source and environmental characteristics are assumed to be known and a solution for the received field is desired. The two major assumptions for both the direct and inverse solutions are: that the source is concentrated at a single point in space in an ocean with cylindrical symmetry, and that the sound speed is allowed to vary arbitrarily with depth but is invariant with range.

It is well known that the field can be obtained by performing a Fourier synthesis over frequency of the product of $H(r,z,f)$; the transfer function of the medium, and $F(f)$, which is the spectrum of the source waveform. It is also well known that the transfer function can be expressed as the Fourier-Bessel transform given by the bottom equation where G is the depth dependent Green's function which contains all of the information about the environment.

Both of the integrals can be numerically evaluated using the discrete fast Fourier transform, commonly known as the FFT. The evaluation of the first equation is rather straightforward, but the second requires some explanation.

The transfer function given in figure 2 is first rewritten in terms of the Hankel function corresponding to outward propagating waves. The key observation is that if the large argument asymptotic approximation, given by the second equation, is substituted for the Hankel function $H_0^{(1)}$, the transfer function is then given by the Fourier type integral shown on the third line. It should be noted that the range of integration is relatively quite small since it is related to the minimum sound speed of the problem. We have included the parameter ϵ to indicate that in practice we integrate to a slightly larger wave number to insure that evanescent waves are also included.

The third equation is then numerically evaluated using the FFT for each discrete frequency of interest to provide the transfer function of the medium as a function of both range and frequency at a given source and receiver depth. Multiplication by the source spectrum and the evaluation of another FFT then yields the received waveform as a function of range and time.

The success experienced with this approach led us to consider the possibility of inverting the entire process.

We define the inverse solution given in figure 3, as that situation where the source characteristics and received signal, as a function of range, are assumed to be known and information about the environment is desired. In particular, the information sought is the impedance at the water bottom interface as a function of wave number.

The inverse solution is obtained by first performing a deconvolution (i.e., taking the ratio of the Fourier transform of the output to the input) and then taking the inverse Bessel transform over horizontal range to give us the depth dependent Green's function versus the horizontal component of the wave number. Since this function depends on the properties of the medium, it

is possible to carry the process one step further and solve for the impedance at the water bottom interface under the assumption that you know the sound speed to that depth.

Before proceeding to the examples let's examine the inversion of the transfer function itself shown by the first equation, in figure 4. As before use is made of the asymptotic expression for the Hankel function to yield the Fourier type integral on the second line. The effect of this approximation is minimal and will be illustrated in the examples. As can be seen from the last equation, the approximate Green's function is given by the convolution of the exact Green's function with the Fourier transform of the range window which extends from 0 to R_{MAX}.

Thus, if the inverse result is to be a good approximation to the exact answer over all values of the horizontal wave number, the aperture in range or R_{MAX} must be fairly large. This is in contrast to the small wave number aperture ξ_{max} needed in the direct solution. The effects of various range apertures will be graphically presented in the last example to be considered.

It is interesting to note that the approximate inverse solution as given by the middle equation can be considered as the output of a long horizontal line array with a phase delay equal to the horizontal component of the wave number and amplitude shading equal to the square root of the distance from the source.

The results of inverse solution for three problems, figure 5, of successive orders of environmental complexity will be presented. In all cases the direct solution was used to generate the received pressure field. Thus, the exact answer for the inverse solution is known in advance and these results serve as a check on the computations and as an illustration of the effects of using a limited range aperture.

The first case is the simplest possible example. The ocean is infinite and of constant sound speed with a CW signal as the input waveform. The direct path will be inverted to obtain the total depth dependent Green's function.

The next case is slightly more complicated since a high speed half space has been inserted and the input waveform is a pulsed CW. The portion of the field containing the reflected and lateral waves will be inverted to first yield the total Green's function and from that the solution for the Rayleigh plane wave reflection coefficient.

The last example is the most complicated environment that can be considered under the initial assumption of range invariance. The sound speed profile was taken from a deep water site in the North Atlantic, and numerous multipaths are present in the received signal. The received pressure field for an infinite CW input waveform will be inverted to produce the total depth dependent Green's function.

The exact inverse solution for the case of only a direct path is given by the first equation in figure 6. It should be noted that it is necessary to include attenuation, represented by the parameter d in the received field, in order to achieve a practical range aperture.

The Bessel transform on the right was evaluated by using the FFT technique discussed earlier. The associated parameters are shown on the bottom of the figure. The calculation yields values of the Green's function for wave numbers from ξ_o to ξ_{max} which is larger than the free space wave number k_1.

The inverse solution for the depth dependent Green's function and the exact answer are shown in figure 7, plotted versus the horizontal component of the wave number. The agreement is excellent (the two curves over plot exactly except for values of the horizontal component of the wavenumber less than .01. The heavy line is the IFFP solution.) except for very small values of the wave number which correspond to small angles as measured from the vertical. For these angles the horizontal range would also be small and in the limiting case of the receiver directly over the source both would be zero. Thus, the product of the two quantities is also small and violates the large argument assumption used to approximate the Hankel function. This limitation can be avoided by evaluating the Bessel transform with a FFT but in a slightly different manner. This has been done, but the lack of time does not permit a more detailed explanation.

The received waveforms for the second example as calculated by the direct solution for only the bottom interfacing portion of the field are shown in figure 8 for three ranges. From left to right they correspond to a range prior to the critical range where the grazing angle is 39.6^o, and is greater than the critical angle. At this range only the reflected wave exist; next for a range just beyond the critical range where the grazing angle is 31.7^o and slightly smaller than the critical angle. At this range both the reflected and lateral waves exist but are coincident in time; and finally at a range well beyond the critical range where the grazing angle is 6.8^o and the two waves are separated in time. These signals and those at other ranges were then used as input values for the inverse solution.

The right-hand side of the equation in figure 9 is evaluated numerically by first taking the FFT over time of the received waveforms at each range point which gives the function script G under the integral. The Bessel transform is then evaluated by the FFT over range to provide values for the depth dependent Green's function appearing on the left-hand side of the equation versus wave number. Since the analytic expression for G, given by the second equation, is known, we can then solve for the Rayleigh plane wave reflection coefficient, $V(\xi)$.

Before looking at those results. it should be noted that the maximum range of integration used in this example corresponds to an incident angle of 83^o so that the range aperture is truncated and some aliasing in the final result is expected.

The absolute magnitude of the inverse solution and the exact answer are plotted versus the angle of incidence in figure 10. It is evident that excellent agreement exist everywhere except for small angles less than 2^o, and for large angles greater than 75^o. Small angles of incidence are associated with small values of horizontal range, thus the product of the horizontal component of the wave number and range is also small; and this violates the large argument assumption used in approximating the Hankel functions.

The oscillation at the large angles of incidence is due to the aliasing introduced by taking a truncated range aperture.

For the last example to be discussed, figure 11, a 24 Hz infinite CW source was located at a depth of 325 ft (99 m) in a deep surface duct and the receiver was deep in the water column at 15,900 ft (4846 m). The depth of the water was 17,400 ft (5303 m) and the bottom was assumed to be a fast constant sound speed half space. The inverse solution is used to solve for the total depth dependent Green's function. It is possible to take the solution one step further as was done in the previous example and solve for the impedance at the ocean bottom, but although the formulas have been worked out the numerical calculations have not been done to date.

In discussing the required range resolution and aperture (see figure 12) it is helpful to recall that the transfer function can be expanded in a normal mode series. Each term in the series is periodic with range but the periods are not harmonically related. The terms which oscillate the fastest or equivalently have the smallest skip distance correspond in this case to steep angle bottom bounce paths. The range resolution must be chosen small enough so that a sufficient number of spatial samples are obtained over a complete cycle of these paths. For all of the results to be shown Δr was held constant at 1700 ft (518 m). Because of the FFT relationship the extent of the wave number aperture given by the expression in the upper right-hand corner is inversely proportional to the range resolution.

The maximum range to which field values must be taken is related to those paths which have the longest skip distance. In this example they are the convergence zone paths. If useful information about these wave numbers is desired then field values are needed over a complete cycle, which would be the distance to two convergence zones.

Results will be shown for two different range apertures. The first denoted by 4096 points equals a maximum range in excess of 33 convergence zones. The second having 256 points extends slightly beyond the second convergence zone.

The extent of the range aperture then determines the wave number resolution as can be seen from the expression in the lower right-hand corner. The 256 point aperture results in a larger value for $\Delta\xi$ and thus less resolution.

A comparison is shown in figure 13 between the absolute magnitude of the Green's function for the exact and inverse solutions versus the horizontal component of the wave number. For the range aperture corresponding to 4096 points, the wave number resolution is small enough ($= 9.023420 \times 10^{-7}$) so that the peaks which correspond to the location of the normal mode eigenvalues are well defined. This is especially true in that portion of the plot corresponding to the bottom bounce (wavenumbers less than approximately .0297) energy where the height of the peaks agree very well. The height of the peaks do not agree as well in the RSR (wavenumbers greater than approximately .0297) region but it is difficult to see the difference in this presentation.

The only difference between the result in figure 14 and that for the previous figure is that the number of range points has been reduced from 4096 to 256. Thus the range aperture has been reduced from slightly larger than 33 convergence zones to slightly greater than 2. This results in a decrease in

the wave number resolving power (= 1.443730×10^{-5}) by a factor of 16. As a consequence almost all of the peaks located to the right of the slide corresponding to RSR paths have been missed. However, we are still doing quite well in the bottom bounce region to the left. It is this region which interests us since the impedance of the bottom for these angles is the quantity for which we eventually wish to solve.

The previous two figures provide some indication of the error introduced by decreasing the range aperture. Additional insight can be obtained by comparing the relative error between the exact and inverse solution at only those points where the computed inverse solution exist. Those results are shown in figure 15 for both the 4096 (the curve which starts with positive values) and 256 range apertures. It can be seen that the relative errors associated with the two range apertures are similar for all wave numbers and both do very well in the bottom bounce region.

Thus the smaller aperture results in a decrease in the wave number resolution power and causes us to miss information related to the RSR peaks, however, the solution captures the peaks in the bottom bounce region and also gives excellent agreement for those wave numbers in the RSR region where the inverse solution exist.

Summary

We are encouraged by the success of our results to date, however, many questions remain to be answered before the scheme can be considered practical. The effect which a limited range aperture has on the determination of the impedance and not merely the depth dependent Green's function clearly must be determined. Also only simulated data with no ambient noise has been used to date, and the real test of the practicality of the inverse solution will come when it is applied to actual experimental data.

Direct Solution

- Source Characteristics and Environment Given
- Solution for Received Pressure Field vrs Range Desired

$$\tilde{p}_R(r,z,t) = \int_{-\infty}^{\infty} \underbrace{H(r,z,f)}_{\text{Transfer Function}} \underbrace{F(f)}_{\text{Source Spectrum}} e^{-i2\pi ft}\, df$$

$$H(r,z,f) = \int_0^{\infty} 2G(z_s,z;\xi,f) J_0(\xi r)\, \xi\, d\xi$$

FIGURE 1

Direct Solution - Evaluation of Bessel Transforms

$$H(r,3,f) = \int_0^\infty G(3_s,3;\xi,f)\, H_o^{(1)}(\xi r)\, \xi\, d\xi$$

$$H_o^{(1)}(\xi r) \sim A^+ e^{i\xi r}/\sqrt{\xi r} \qquad (\xi r) >> 1$$

$$H(r,3,f) \sim A^+/\sqrt{r} \int_0^{\xi_{max}} G(3_s,3;\xi,f)\sqrt{\xi}\, e^{i\xi r}\, d\xi$$

Integration Aperture Small

$$0 \le \xi \le \xi_{max} = 2\pi f/c_{min} + \epsilon$$

FIGURE 2

- Source Characteristics, Received Signal Given
- Information About Environment Desired

Deconvolution

$$\int_0^\infty 2G(z_s,z;\xi,f)J_0(\xi r)\xi\,d\xi = \mathcal{U}(r,z,f)/F(f)$$

$$\mathcal{U}(r,z,f) = \int_{-\infty}^{\infty} \tilde{P}_R(r,z,t)e^{i2\pi ft}dt$$

Bessel Transform on Range

$$2G(z_s,z;\xi,f) = \left[\int_0^\infty \mathcal{U}(r,z,f)J_0(\xi r)r\,dr\right]/F(f)$$

$G(z_s,z;\xi,f)$ A Function of Bottom Impedance

FIGURE 3

Inverse Solution (Range Aperture)

$$G(\zeta_s, \zeta; \xi, f) = \int_0^\infty \frac{H(r, \zeta, f)}{4} H_0^{(2)}(\xi r)\, r\, dr$$

$$G_a(\zeta_s, \zeta; \xi, f) \sim A^- / \sqrt{\xi} \int_0^{R\max} \frac{H(r, \zeta, f) e^{-i\xi r}}{4} \sqrt{r}\, dr$$

$$G_a(\zeta_s, \zeta; \xi, f) \sqrt{\xi} \sim \frac{1}{2\pi} \int_0^{\xi_{max}} G(\zeta_s, \zeta; \mu, f) \frac{\sin\left[\frac{\mu - \xi}{2}\right] R\max}{\left[\frac{\mu - \xi}{2}\right]} e^{i\left(\frac{\mu - \xi}{2}\right) R\max} d\mu$$

TM No. 77260

FIGURE 4

Examples: Inverse Fast Field Program

- Infinite constant sound speed ocean (single path CW)

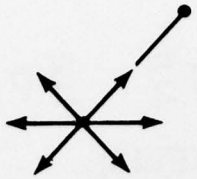

- semi-infinite ocean constant SSP (two paths-pulsed CW)

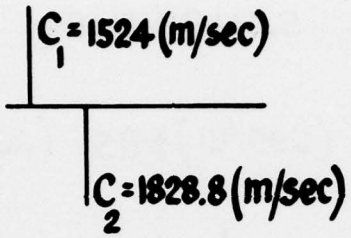

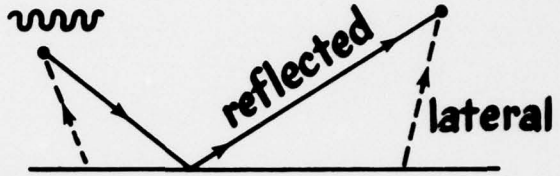

- North Atlantic SSP (numerous multipath-CW)

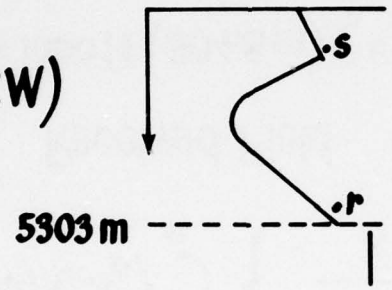

FIGURE 5

Single Path Infinite CW

$$G(3_s,3;\xi,f_o)-G^*(3_s,3;\xi,f_o)=\int_o^\infty\left\{\frac{\sin(k,R)}{R}e^{-dR}\right\}J_o(\xi r)r\,dr$$

Received Field

$3 = 2000\,ft\,(609.6\,m)\quad 3_s = 1000\,ft\,(304.8\,m)\quad f_o = 50\,Hz\quad d = 10^{-4}\,Nepers/ft$

$$G(3_s,3;\xi,f_o)=\frac{ie^{\lambda(3-3_s)\beta}}{2\beta}\qquad \beta=\sqrt{k_1^2-d^2-\xi^2+2ik,d}$$

$C_1 = 5000\,(ft/sec)\quad 1524\,(m/sec)$

FFT Parameters

$N = 8192\quad f = 50\,Hz$

$r_o = 25\,ft\qquad \Delta r = 25\,(ft)\qquad R\max = 204{,}800\,ft$

$A\xi = .30679616\times10^{-4}\qquad \xi_o = \Delta\xi\qquad \xi\max = .12566$

FIGURE 6

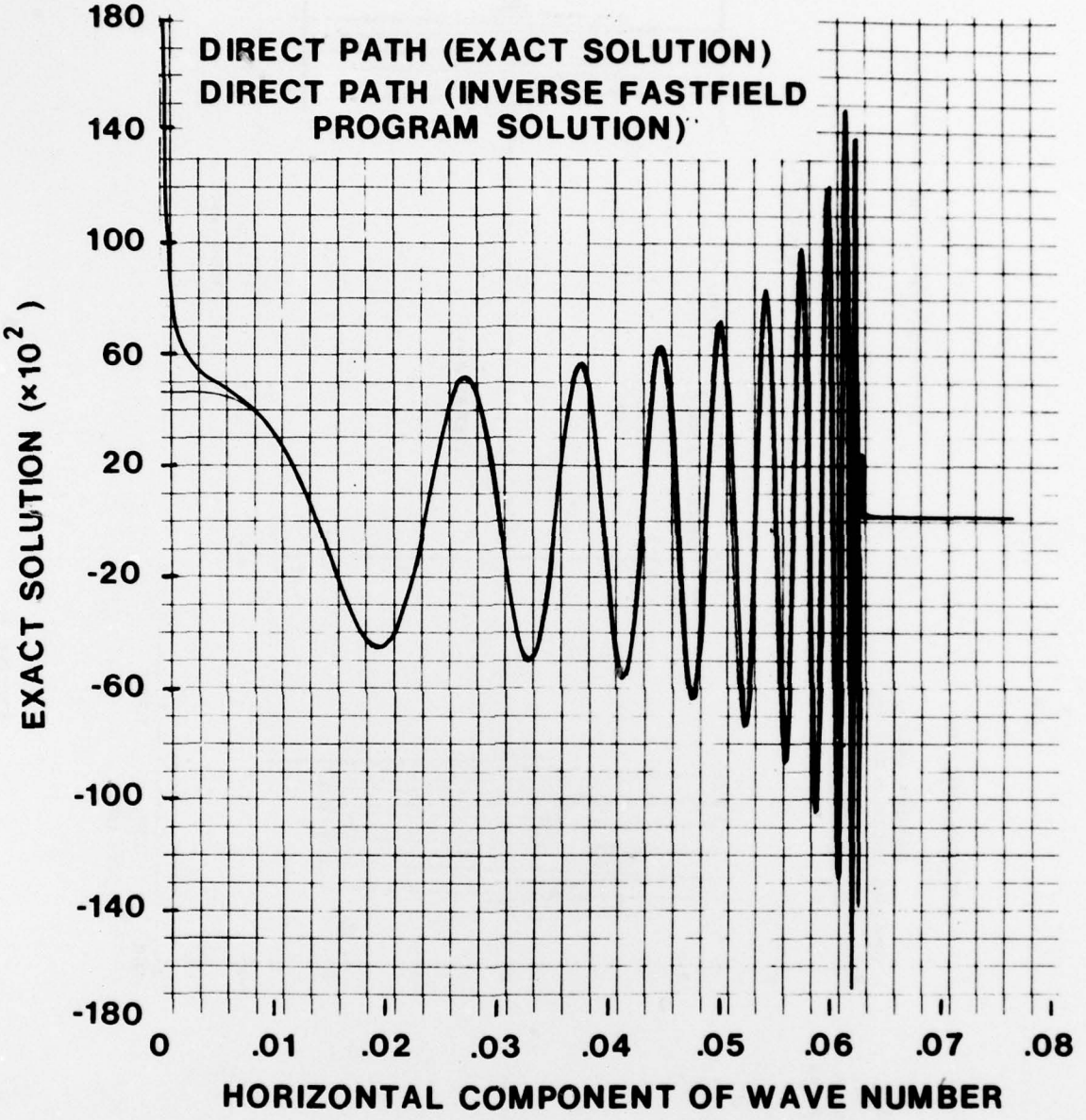
DIRECT PATH (EXACT SOLUTION)
DIRECT PATH (INVERSE FASTFIELD PROGRAM SOLUTION)
EXACT SOLUTION (×10²)
180
140
100
60
20
-20
-60
-100
-140
-180
0
.01
.02
.03
.04
.05
.06
.07
.08
HORIZONTAL COMPONENT OF WAVE NUMBER

FIGURE 7

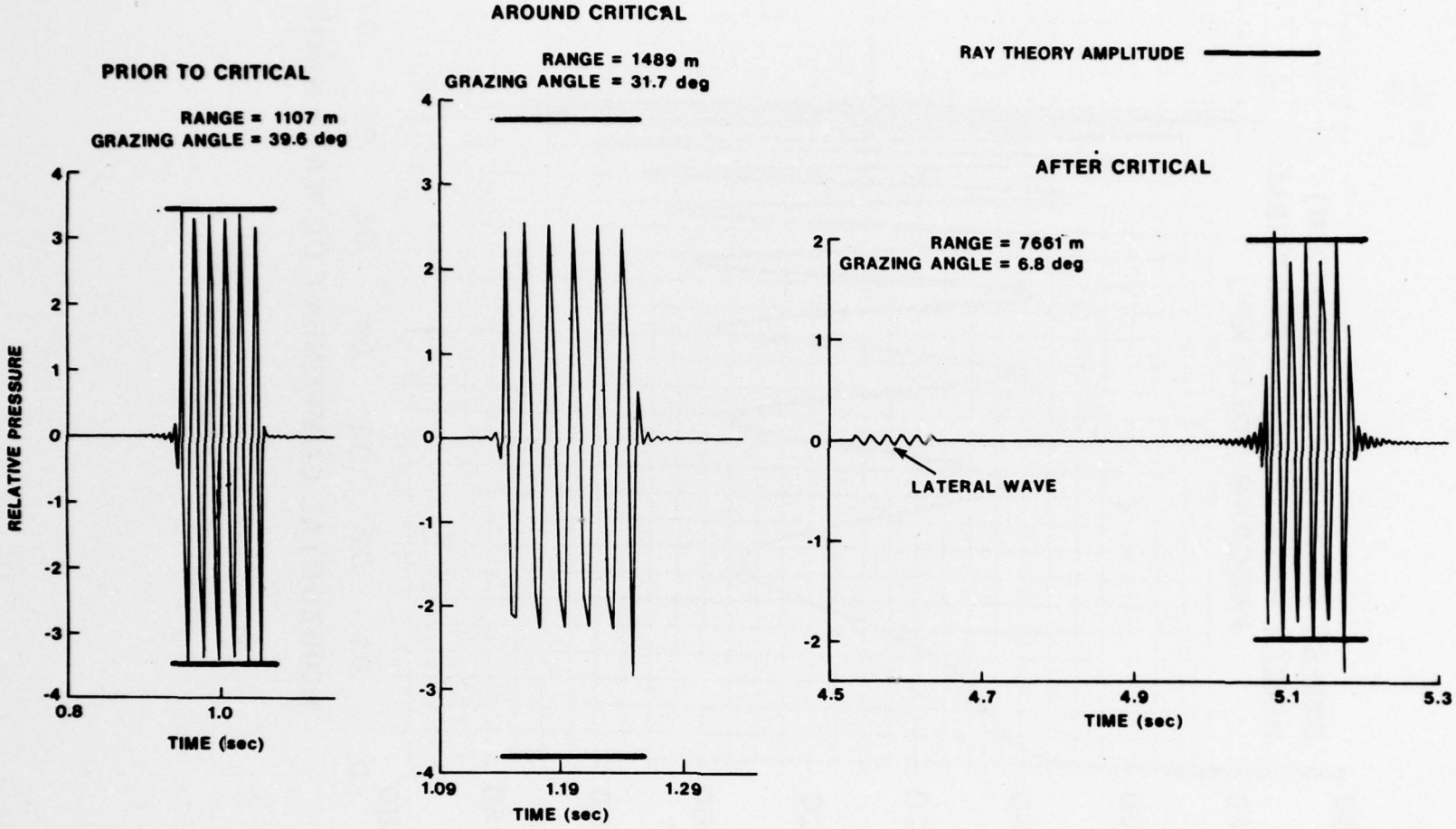
PRIOR TO CRITICAL
RANGE = 1107 m
GRAZING ANGLE = 39.6 deg
RELATIVE PRESSURE
TIME (sec)
AROUND CRITICAL
RANGE = 1489 m
GRAZING ANGLE = 31.7 deg
TIME (sec)
RAY THEORY AMPLITUDE
AFTER CRITICAL
RANGE = 7661 m
GRAZING ANGLE = 6.8 deg
LATERAL WAVE
TIME (sec)

FIGURE 8

Inverse Solution (two paths - pulsed CW)

$$G(z_s, z; \xi, f) = \left[\int_0^{\infty} \mathcal{H}(r, z, f)\, J_0(\xi r)\, r\, dr\right] / F(f)$$

$$G(z_s, z; \xi, f) = \frac{i V(\xi) e^{i(z+z_s)\beta}}{2\beta}$$

$r_o = 24.54$ ft

$\Delta r = 24.54$ ft

$R_{max} = 25{,}132.74$ ft

$N = 1024$

$\xi_o = .625 \times 10^{-4} (ft)^{-1}$

$\Delta \xi = .250 \times 10^{-3} (ft)^{-1}$

$\xi_{max} = .2560625 (ft)^{-1}$

$f = 49.804687$ Hz

FIGURE 9

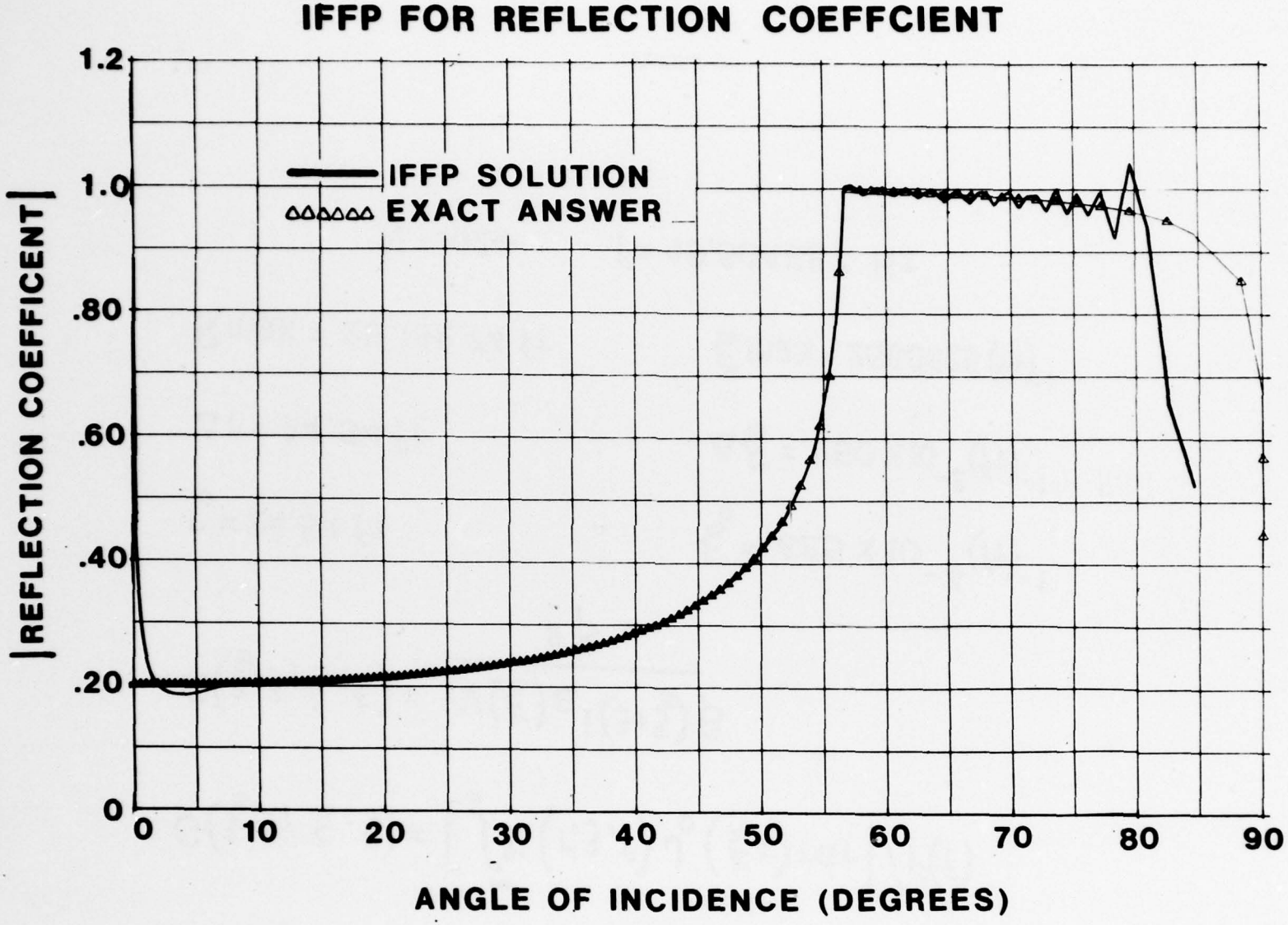

FIGURE 10

North Atlantic SSP
numerous multipath-infinite CW(24 Hz)

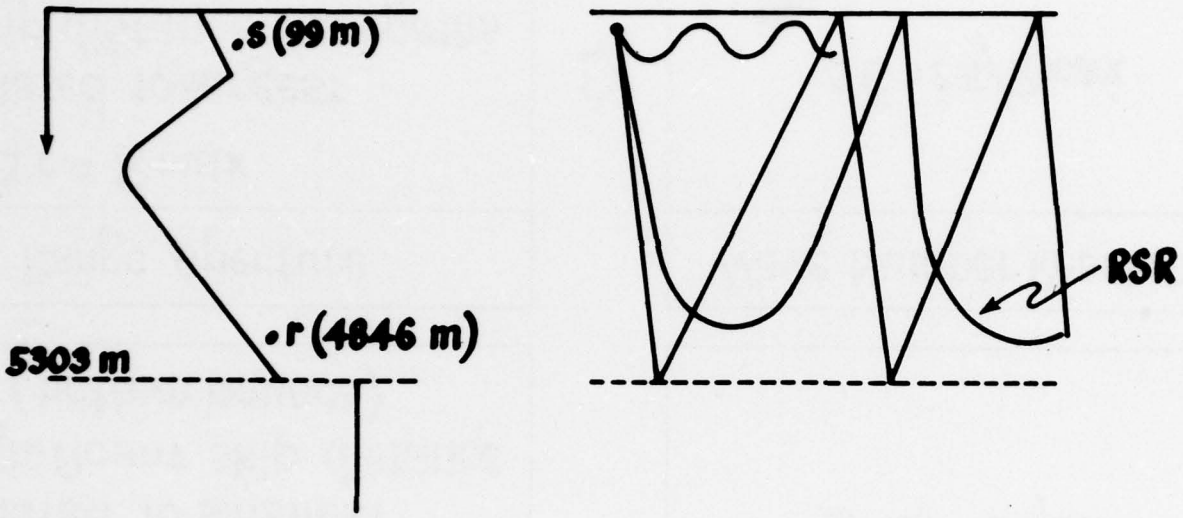

FIGURE 11

$$H(r,\zeta,f) \sim \Sigma_k \phi(\zeta,\xi_k) e^{i\xi_k r}/\sqrt{r}$$

Range Resolution		Wave Number Aperture
$\Delta r = 1700\,ft\ (\sim 518\,m)$ Related to smallest significant skip distance (bottom bounce)	⇨	$\xi_{max} = 2\pi/\Delta r$

Range Aperture		Wave Number Resolution
$N\Delta r = R_{max}$ Related to largest skip distance (CZ) paths 4096 pts. $N\Delta r$ = 1,160.5 nmi 256 pts. $N\Delta r$ = 72.53 nmi	⇨	$\Delta\xi = 2\pi/R_{max}$

TM No. 77160

FIGURE 12

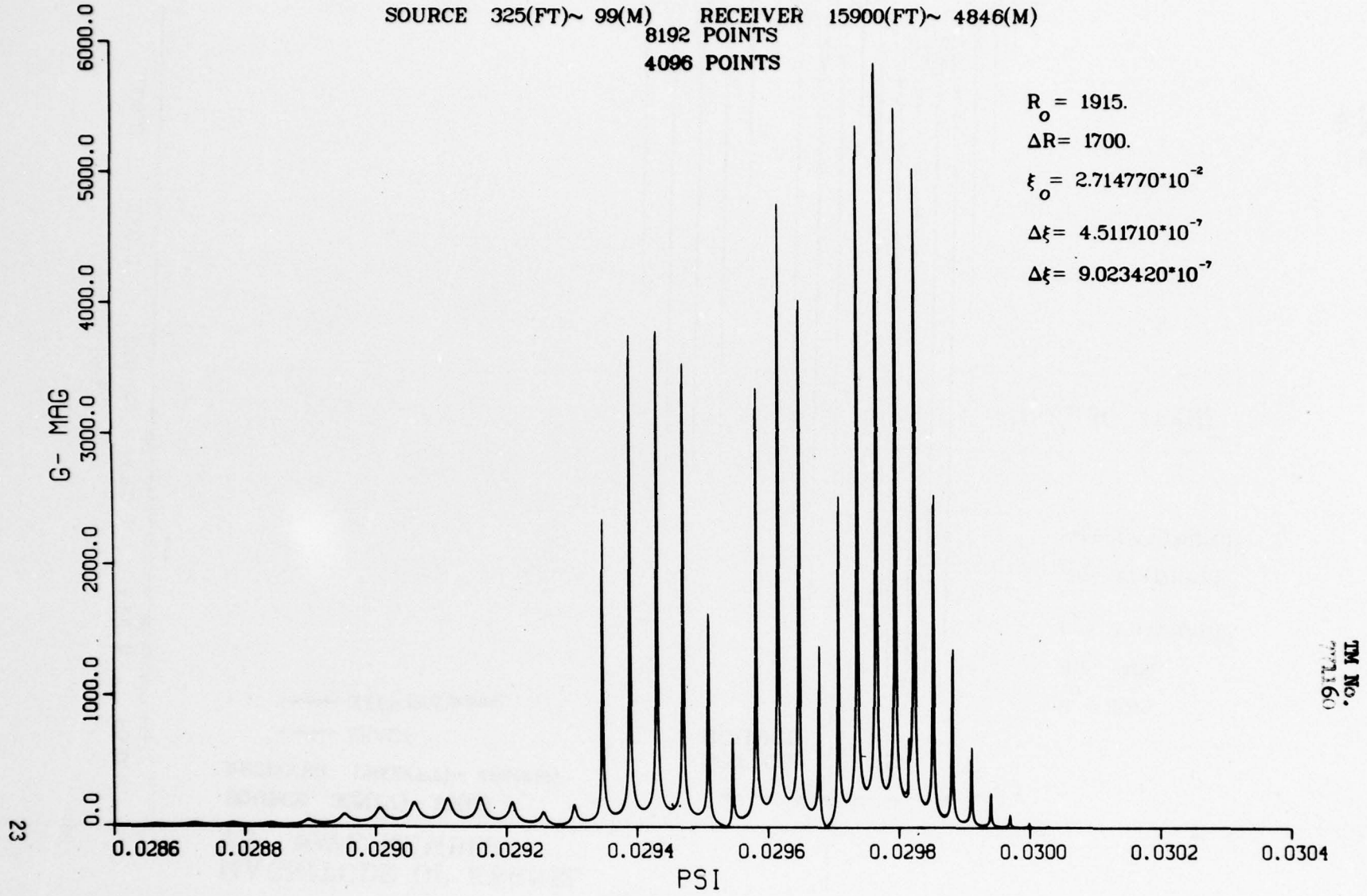

FIGURE 13

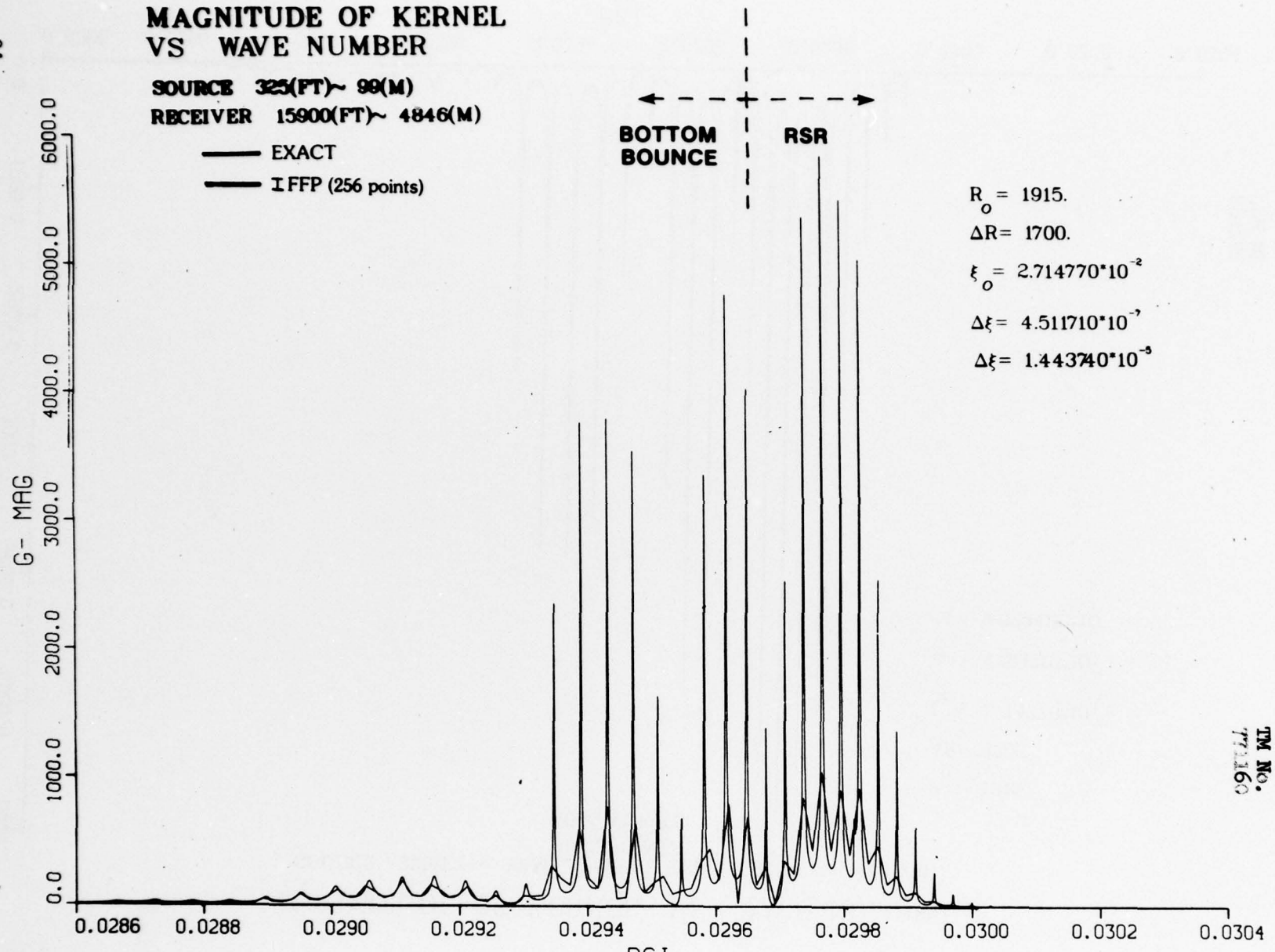
MAGNITUDE OF KERNEL
VS WAVE NUMBER
SOURCE 325(FT)~ 99(M)
RECEIVER 15900(FT)~ 4846(M)
EXACT
IFFP (256 points)
BOTTOM BOUNCE
RSR
R_o = 1915.
ΔR= 1700.
ξ_o = 2.714770*10^-2
Δξ= 4.511710*10^-7
Δξ= 1.443740*10^-5
G- MAG
0.0
1000.0
2000.0
3000.0
4000.0
5000.0
6000.0
0.0286
0.0288
0.0290
0.0292
0.0294
0.0296
0.0298
0.0300
0.0302
0.0304
PSI

FIGURE 14

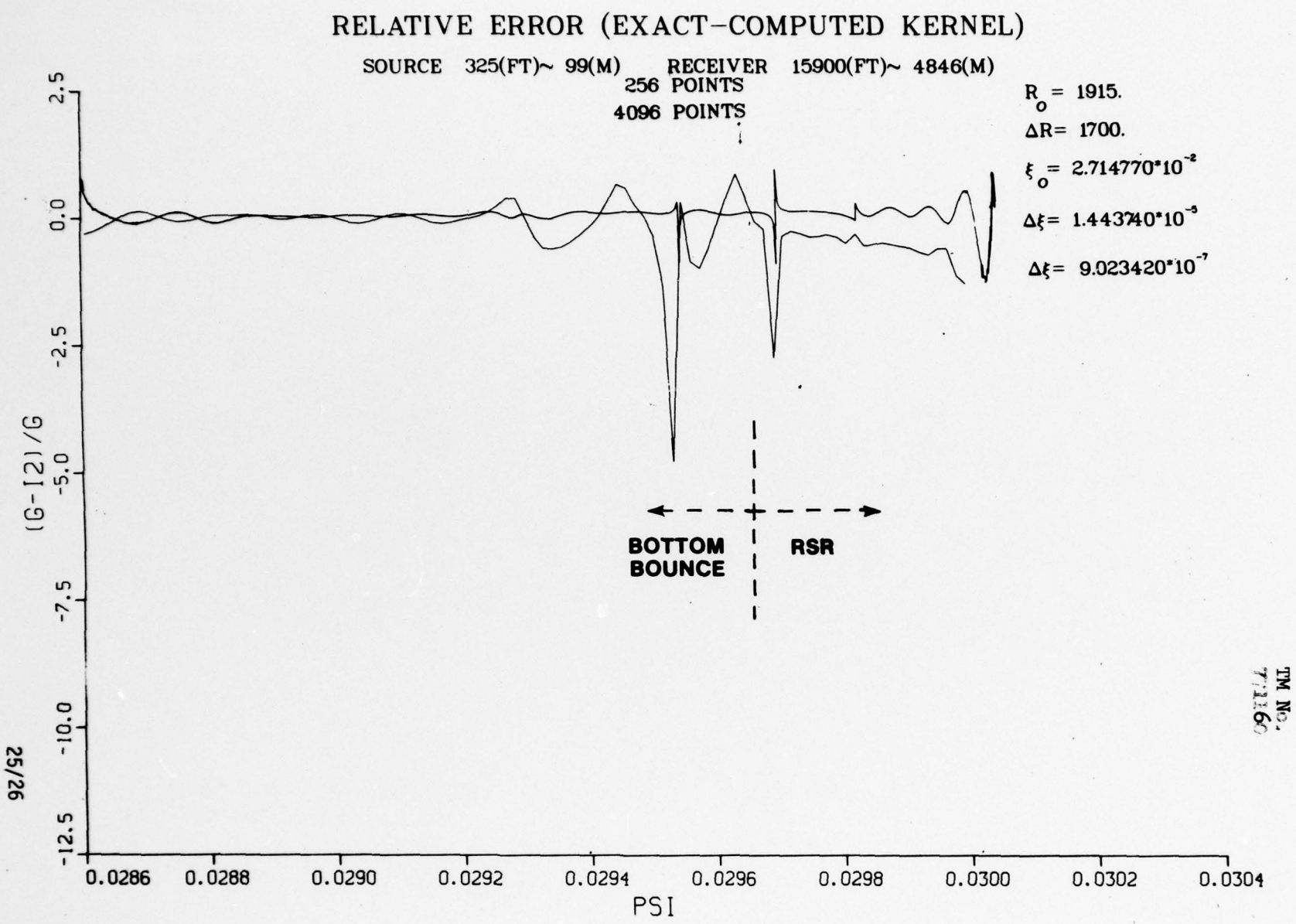

FIGURE 15

THE INVERSE FAST FIELD PROGRAM (IFFP): AN APPLICATION TO THE DETERMINATION OF THE ACOUSTIC PARAMETERS OF THE OCEAN BOTTOM

F.R. DiNapoli
Special Projects Department

TM No. 771160
5 August 1977
UNCLASSIFIED

DISTRIBUTION LIST

External

Tel-Aviv University, Dept. of Geophysics, Tel Aviv, Israel (M. Schoenberg)

Delft University of Technology, Physics Dept., Lorentzbug 1, Delft, The Netherlands (A. Berkhant)

Brodarski Institute, Frouse 1, 91000 Zagreb, Yugoslavia (J. Ivica)

Forschungsanstalt der Bundeswehr, fuer Wasserschall-und Geophysik, Klausdorfer Weg 2-24, D-2300, Kiel 14, FGR (H. Schneider)

Weapons Research Establishment, Box 2151, G.P.O. Adelaide 5001 Australia (G. Gartrell)

Academy of Sciences of USSR, Leninskii, Prospect 14, Moscow 117071 (L. Brekhovskikh)

SACLANT ASW RESEARCH CENTRE (F. Jensen, W. Kuperman)

Defense Research Establishment Atlantic, Canada (H. Merlinger)

Defense Research Establishment Pacific, Canada (D. Thomson)

NAVSEA (SEA 06H1-4, A. Franceschetti)

NRL (Code 8120, F. Ingenito, J. DeSanto, O.I. Diachak)

NOSC (Code 573 H. Bucker, Code 503 D. Gorden, Code 503 M. Pederson, Code 308 J. Stewart)

NAIDC (C. Bartberger)

Naval Surface Weapons Center (I. Blastein)

NORDA (H. Bezdek, A. Anderson Code 320)

ARL Penn State (D. Stickler, S. McDaniel)

Southeastern Mass. University, Electrical Engineering Dept. (G. Fain, L. Estes)

ARL University of Texas (G. Bardin)

H.W. Marsh, Box 226, Penrose, NC 28766

Lamont-Doherty Geological Observatory, Palisades NY (H. Kutschale, P. Stoffa, P. Richards)

Courant Institute of Math. Sciences, NYU (F. Tappert)

D. Hyde, Assistant Secretary of the Navy, (R&D), Washington, D.C. 20350

DISTRIBUTION LIST (Cont'd)

External

J. Pierre Lefebvre, Laboratoire de Mecanique et d'Acoustique
31, Chemin Joseph-Aiguier (9e Arr.) 13 274 Marseille Cedex 2, France

M. West, Dept. of Applied Acoustics, University of Salford, Salford M5 4NT England

N. Bleistein, Dept. of Mathematics, University of Denver, Denver, CO

DARPA (Code TTO Capt H. Cox)

Asst. Dir. Land Resources U.S. Geological Survey (J. Balsley)

AMOCO Production Company, P.O. Box 591, Tulsa, OK 74102 (J. Domenico)

D. Feit, B. Vogel, Code 934 NSRDC, Bethesda, MD 20084

N. Bojarski, Sixteen Pine Valley Lane, Newport Beach, CA 92660

TRACOR (R. Urick)

Internal

01	(C. Pryor)
10	(W. VonWinkle)
	(P. Stocklin)
101	(E. Eby, D. Viccione, A. VanWoerkom)
222	(G. Leibiger)
31	(R. Hasse)
312	(D. Browning, R. Deavenport, F. DiNapoli (20), R. Dullea, P, Herstein, E. Jensen, D. Lee, W. Roderick, S. Santaniello, W. Schumacher)
3123	(R. Lauer, D. Wood, J. Papadakis)
313	(P. Abraham, P. Cable, M. Lackoff, R. Mellen, A. Nuttall, H. Quazi)
314	(J. Cohen, T. Einstein, H. Weinberg)
4502	(R. Bernier)
45552	(10 copies)
542	(3 copies)
5421	

External: 44 copies
Internal: 64 copies
Total: 108 copies